Title: Intrinsic excitation-inhibition imbalance affects medial prefrontal cortex differently in autistic men versus women

Authors: Stavros Trakoshis[1,2], Pablo Martínez-Cañada[3,4], Federico Rocchi[5], Carola Canella[5], Wonsang You[6], Bhismadev Chakrabarti[7,8], Amber N. V. Ruigrok[7], Edward T. Bullmore[9,10], John Suckling[10], Marija Markicevic[11], Valerio Zerbi[11,12], MRC AIMS Consortium†, Simon Baron-Cohen[7,9], Stefano Panzeri[3]*, Alessandro Gozzi[5]*, Meng-Chuan Lai[7,13,14,15,16]*, & Michael V. Lombardo[1,7]*

Affiliations:

1 Laboratory for Autism and Neurodevelopmental Disorders, Center for Neuroscience and Cognitive Systems @UniTn, Istituto Italiano di Tecnologia, Corso Bettini, 31, 38068 Rovereto, Italy
2 Department of Psychology, University of Cyprus, Nicosia, Cyprus
3 Neural Computation Laboratory, Center for Neuroscience and Cognitive Systems @UniTn, Istituto Italiano di Tecnologia, Corso Bettini, 31, 38068 Rovereto, Italy
4 Optical Approaches to Brain Function Laboratory, Department of Neuroscience and Brain Technologies, Istituto Italiano di Tecnologia, Via Morego 30, 16163 Genova, Italy
5 Functional Neuroimaging Laboratory, Center for Neuroscience and Cognitive Systems @UniTn, Istituto Italiano di Tecnologia, Corso Bettini 31, 38068 Rovereto, Italy
6 Children's National Medical Center, Department of Diagnostic Imaging and Radiology, Washington, DC, USA
7 Autism Research Centre, Department of Psychiatry, University of Cambridge, Cambridge, United Kingdom
8 Centre for Integrative Neuroscience and Neurodynamics, School of Psychology and Clinical Language Sciences, University of Reading, Reading, United Kingdom
9 Cambridgeshire and Peterborough National Health Service Foundation Trust, Cambridge, United Kingdom
10 Brain Mapping Unit, Department of Psychiatry, University of Cambridge, Cambridge, United Kingdom
11 Neural Control of Movement Lab, D-HEST, ETH Zurich, Auguste-Piccard-Hof 1, 8093 Zurich, Switzerland
12 Neuroscience Center Zurich, University and ETH Zurich, Winterthurerstrasse 190, 8057 Zurich, Switzerland
13 The Margaret and Wallace McCain Centre for Child, Youth & Family Mental Health, Azrieli Adult Neurodevelopmental Centre, and Campbell Family Mental Health Research Institute, Centre for Addiction and Mental Health, Toronto, Canada
14 Centre for Brain and Mental Health and Department of Psychiatry, The Hospital for Sick Children, Toronto, Canada
15 Department of Psychiatry, Faculty of Medicine, University of Toronto, Toronto, Canada
16 Department of Psychiatry, National Taiwan University Hospital and College of Medicine, Taipei, Taiwan

* Equal contributions

Corresponding Author: Michael V. Lombardo (michael.lombardo@iit.it)

† MRC AIMS Consortium Author List (Alphabetical Order)

Anthony J. Bailey (Oxford), Simon Baron-Cohen (Cambridge), Patrick F Bolton (IoPPN), Edward T. Bullmore (Cambridge), Sarah Carrington (Oxford), Marco Catani (IoPPN), Bhismadev Chakrabarti (Cambridge), Michael C. Craig (IoPPN), Eileen M. Daly (IoPPN), Sean C. L. Deoni (IoPPN), Christine Ecker (IoPPN), Francesca Happé (IoPPN), Julian Henty (Cambridge), Peter Jezzard (Oxford), Patrick Johnston (IoPPN), Derek K. Jones (IoPPN), Meng-Chuan Lai (Cambridge), Michael V. Lombardo (Cambridge), Anya Madden (IoPPN), Diane Mullins (IoPPN), Clodagh M. Murphy (IoPPN), Declan G. M. Murphy (IoPPN), Greg Pasco (Cambridge), Amber N. V. Ruigrok (Cambridge), Susan A. Sadek (Cambridge), Debbie Spain (IoPPN), Rose Stewart (Oxford), John Suckling (Cambridge), Sally J. Wheelwright (Cambridge) and Steven C. Williams (IoPPN).

Abstract

Imbalance between neurophysiological excitation versus inhibition (E:I) has been theorized as a core pathophysiological mechanism of autism. However, a majority of the evidence behind the E:I theory comes from animal models of rare genetic mutations that account for only a small fraction of the autistic population. Scale-free metrics of neural time-series data could represent biomarkers for E:I imbalance and could enable a greater understanding of how E:I imbalance affects different types of autistic individuals and how such mechanisms relate to behavior. Here we show that a measure of scale-free dynamics, the Hurst exponent (H), measured *in-vivo* in resting state fMRI (rsfMRI) data, is a surrogate marker of E:I imbalance and differentially affects autistic males versus females. *In-silico* modeling of local field potentials (LFP) from recurrent networks of interacting excitatory and inhibitory neurons shows that increasing the E:I ratio by specifically enhancing excitation attenuates H and flattens the 1/f slope. These *in-silico* predictions are confirmed *in-vivo* with chemogenetic manipulations to enhance excitation of prefrontal cortex in mice. In humans, social brain areas such as ventromedial prefrontal cortex (vMPFC), show decreased H specifically in autistic males but not females. However, continuous variation in vMPFC H correlates with ability to behaviorally camouflage social-communicative difficulties in autistic females but not males. This work provides insight into how *in-vivo* neuroimaging readouts can be utilized to understand E:I imbalance in human clinical populations. E:I imbalance in social brain circuitry may differentially affect autistic males versus females and may help explain sex-related differences in compensatory phenomena.

Excitation-inhibition (E:I) balance in the brain has been hypothesized to be atypical in many neuropsychiatric conditions[1,2], including autism. Rubenstein and Merzenich[1] originally suggested that some types of autism may be explained by an E:I imbalance that may lead to hyper-excitability in cortical circuitry and potentially enhanced levels of neuronal noise. However, coming to a better understanding of how E:I balance is affected across a heterogeneous mixture of autistic individuals has proven to be challenging because of the limited availability of robust E:I biomarkers that are non-invasive and applicable in humans and which can be measured on a large scale. A majority of the literature about E:I balance in autism extends from investigations of prominent single gene mutations associated with autism and the animal model research around these genes[2,3]. This leaves a significant gap in evaluating the E:I theory on a larger majority of the autistic population.

While no one theory can fully explain all individuals with an autism diagnosis[4,5], the E:I imbalance theory may have utility for understanding subtypes of autistic individuals[6–8]. Sex/gender may be an important stratifier of relevance for highlighting E:I imbalance subtypes[9,10]. Many highly penetrant autism-associated genes are located on the sex chromosomes (e.g., *FMR1*, *MECP2*, *NLGN3*, *GABRA3*, *ARX*, *SYN1*) and are known to lead to pathophysiology implicating E:I dysregulation[1,11,12]. Other genes playing important roles in the balance between excitation and inhibition in the brain (e.g., *MEF2C, GRIK2, GRIA1, SCN3A, SCN9A, NPTX2*) are highly sensitive to androgens in human neuronal stem cells and are highly expressed in 'social brain' circuitry such as the default mode network, and in particular, the medial prefrontal cortex (MPFC)[13]. Optogenetic stimulation to enhance excitation in mouse MPFC also results in changes in social behavior[14,15]. These results hint that sex-relevant biological mechanisms affect E:I balance and that key social brain regions such as MPFC may be of particular importance for explaining how E:I imbalance affects social behavior.

Sex/gender heterogeneity may also lead to differing clinical presentations and compensatory mechanisms in autism. It is known that many cognitively able adult autistic women engage in camouflaging behaviors that tend to compensate or mask their social-communicative difficulties more so than males[16–18]. Prior work has shown that whereas autistic males show reduced ventral MPFC (vMPFC) self-representation neural response, autistic females show intact vMPFC function. Furthermore, the degree of intact vMPFC self-representation neural activation response in autistic females is associated with enhanced ability to camouflage[19]. If E:I imbalance asymmetrically affects vMPFC function in males more than females, intrinsic E:I neurophysiology could help explain differential camouflaging in adult autistic females.

Scale-free dynamics of neural time-series data measured with non-invasive neuroimaging techniques such as fMRI could represent surrogate markers of E:I imbalance. It has been long known that rsfMRI data exhibits a background of 1/f noise, that is indicative of scale-free characteristics of brain dynamics, such as long memory, self-similarity, and fractality[20–22]. In past work we have shown that one such metric, the Hurst exponent (H), is atypically decreased in rsfMRI data of adult autistic males, particularly for social brain areas like MPFC[23]. H is statistically relevant to neural noise since lower levels of H can be interpreted as closer to what would be expected of a completely noisy random signal (e.g., white noise produces an H = 0.5). At the neurophysiological level, the exponent of the 1/f spectral power law has been recently suggested

to reflect the E:I imbalance[24]. Simulated local field potential (LFP) data based on manipulating directly the E:I ratio show flatter 1/f slopes when E:I ratio is high[24]. Flatter 1/f slopes are related to decreased levels of H[25]. Thus, neurophysiologically heightened E:I ratio generates flatter 1/f slope in LFP data which could drive H (as measured in BOLD) to be decreased.

This work aims to better understand how E:I imbalance may differentially affect autistic males and females. To achieve this aim, we first took a bottom-up approach by using computational models of local neuronal microcircuitry to make *in-silico* predictions about how H and 1/f slope in local field potentials (LFP) and rsfMRI data may behave when there are underlying changes in E:I balance. Importantly, our computational approach takes a major step forward from prior work[24] by utilizing a model that includes interactions within and between excitatory and inhibitory neuronal populations. Our *in-silico* predictions are then tested *in-vivo* with a combination of rsfMRI and chemogenetic manipulations in mice that either increase neurophysiological excitation or that silence the local activity in the network. With this understanding of how scale-free metrics of the neural time-series behave with underlying changes to E:I imbalance, we then turn to the human rsfMRI data to show how E:I imbalance may differ amongst autistic males and females and how such mechanisms may explain individual differences in camouflaging behavior.

Results

In-silico modeling of H in simulated LFP data with modulated E:I ratio or 1/f slope

As a starting point for understanding how scale-free indices such as the1/f slope may be related to E:I mechanisms, we utilized the model reported by Gao and colleagues[24]. In this model, two independent, non-interacting excitatory and inhibitory neuronal populations are simulated and their post-synaptic currents summed into a local field potential (LFP) signal (Figure 1A). When changing the E:I ratio by means of independently varying the strengths of the inhibitory (g_I) and excitatory (g_E) synaptic conductances, we reproduced the primary finding from Gao et al.,[24] that 1/f slope becomes flatter (i.e. less negative) when the E:I ratio in the model becomes larger (Figure 1B). This finding can be explained by the fact that the excitatory AMPA post-synaptic currents have shorter time constants than inhibitory GABA and this leads to a higher frequency power and shallower slope of the excitatory components of the spectrum.

Since 1/f slope is related to H[25], we next computed H from the simulated LFP data. There is a tight relationship between decreasing H and increasing E:I ratio (Figure 1C). Because of this relationship between H and 1/f slope, we next simulated LFP data with prespecified 1/f slopes and then computed H both in the LFP data itself but also when the LFP data is convolved with a canonical hemodynamic response function in order to simulate BOLD signal. Figure 1D shows that H linearly tracks well with 1/f slope in LFP data. In BOLD data, the change in H over 1/f slopes is attenuated relative to how H changes in LFP data. The attenuated change in H in simulated BOLD signal is explained by the fact that the log of power of convolved signal is the sum of the log of the power of the original signal and of the power of the convolution kernel (in our case, the canonical HRF). Given that the additive term of the HRF convolution kernel is the same for all simulated slopes, the convolution with the HRF will flatten out the differences in slopes that are present in the original signal. In sum, the inferences from the Gao model[24] suggest that H can be

utilized as a marker to track changes in E:I balance in LFP and BOLD data. However, H or 1/f slope differences identified in BOLD signal may be strongly attenuated relative to actual differences in those metrics when computed directly on underlying neural time-series represented by the LFP. Thus, changes observed in H in BOLD data can be considered as reflecting true and potentially larger changes in H in the underlying LFP data. In contrast, any lack of change in H measured in BOLD could reflect either a lack of difference within the underlying neural signals or a difference that is too small to survive the convolution with the HRF.

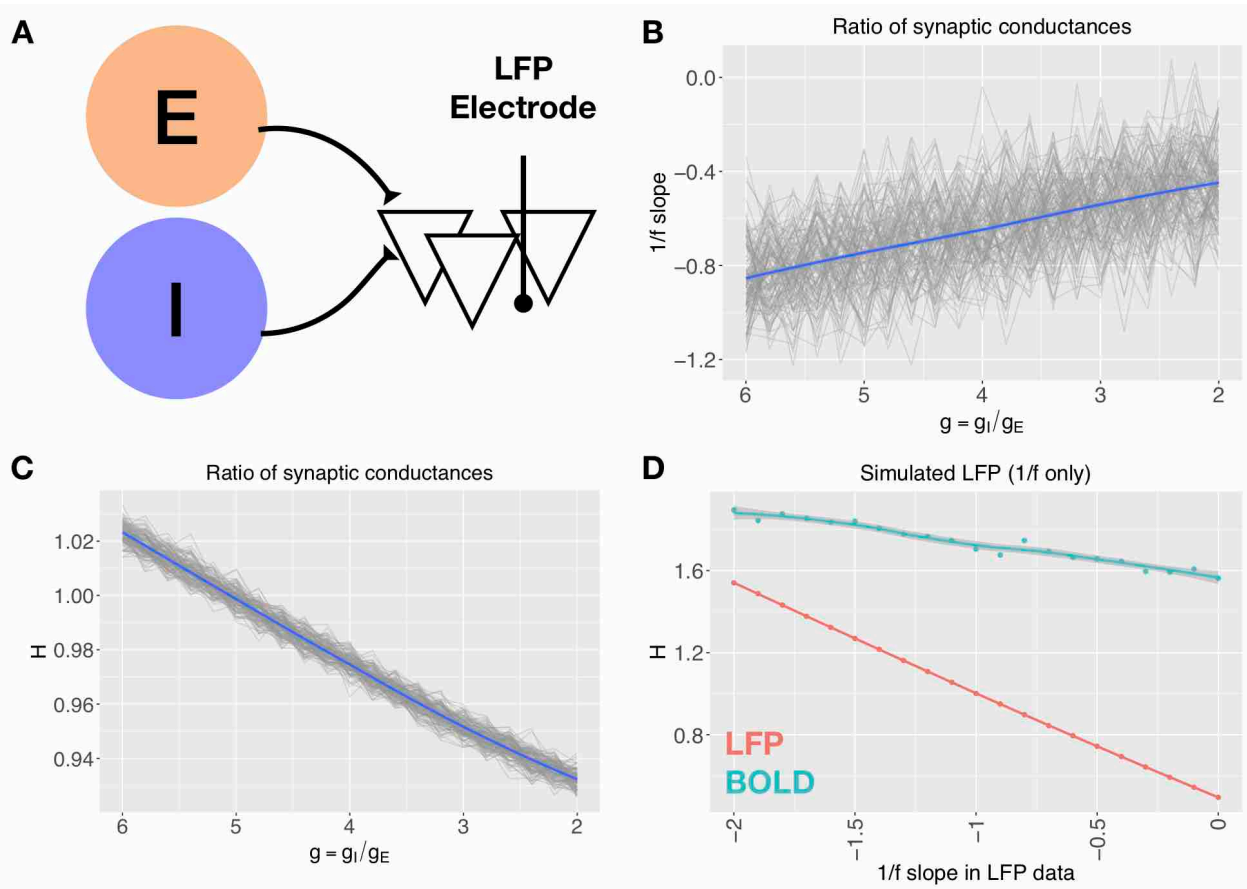

Figure 1: In-silico predictions from a non-recurrent model of how scale-free metrics such as 1/f slope and the Hurst exponent behave when the ratio between excitation and inhibition or 1/f slope in LFP data change. *Panel A shows a schematic of the Gao et al.,*[24] *model that computationally generates LFPs based on manipulated E:I ratios. Panel B reproduces the relationship reported in Gao et al., between 1/f slope and E:I ratio. All 128 simulated channels are shown in gray, and their average is shown in blue. Panel C shows the relationship between H and E:I ratio from the Gao et al., model. Panel D shows H computed on simulated LFP where the 1/f slope is prespecified. H computed on LFP data is shown in pink. H is plotted in cyan when the LFP data is convolved with a canonical hemodynamic response function to simulate BOLD signal.*

Recurrent network modeling of E:I balance

One missing feature of the Gao et al.,[24] model is that it does not include interactions between and within excitatory and inhibitory neuronal populations. These interactions indeed exist

and are fundamental to neural dynamics. For example, an increase in inhibitory conductance will not only affect the power spectral density of inhibitory post-synaptic currents, but will also have a profound influence on the firing of both excitatory and inhibitory neurons. To test whether E:I ratio is linked to changes in 1/f slope and H under this more realistic situation, we simulated a biologically plausible recurrent network model of a canonical cortical circuit incorporating excitatory and inhibitory spiking neurons, that interact through recurrent connections and receive external inputs (both a sensory driven thalamic input and a sensory unrelated intracortical input, see Figure 2A). The model parameters are perturbed starting from a baseline reference set of parameters that set the network in a configuration that has been shown by previous work to capture a large fraction (> 90%) of the variance of LFP across frequencies and stimulus conditions, and to reproduce the information encoding and dynamical properties of the primate visual cortex over a wide range of visual stimulation and spontaneous activity conditions[26–31]. We computed LFP power spectral densities for two levels of strength of thalamic input (υ_0 = 1.5 spikes/second and υ_0 = 2 spikes/second), and we verified that our results hold qualitatively for a wider range of input levels (1.5 to 4 spikes/second). Following established procedures[24,32], we calculated the 1/f slopes over the range in which the spectrum was linear in the log-log plot. This range was 40-70 Hz for a thalamic input of 1.5 spikes/second and 50-80 Hz for 2 spikes/second, see Figure 2B. Interestingly, these frequency ranges are consistent with the gamma frequency range that mostly influences the BOLD signal[33], thereby making in principle these 1/f slope fluctuations particularly detectable in the BOLD signal. Analogous to Gao et al.,[24] first we studied how the 1/f slope varies when modifying the relative ratio between inhibitory (g_I) and excitatory (g_E) conductances ($g = g_I/g_E$). Figure 2C shows flatter slopes if g is reduced (i.e. E:I ratio is increased) from a baseline reference value (g = 11.3) shown in previous studies to reproduce cortical data well. However, an increase in g towards stronger inhibition has weaker effects on the slope, particularly for υ_0 = 2 spikes/second. The 1/f slope values found in our simulations (from -4 to -1) are broadly in agreement with the range of values measured in LFPs and intracranial recordings across species[24,32,34–37]. We next computed H from the same simulated LFPs. Figure 2D confirms the relationship of decreasing H with decreasing g (i.e. increasing E:I ratio) in the regime in which g is smaller than the baseline reference value. If g is greater (i.e. decreasing E:I ratio) than the baseline reference value, we observed that H remained largely unchanged.

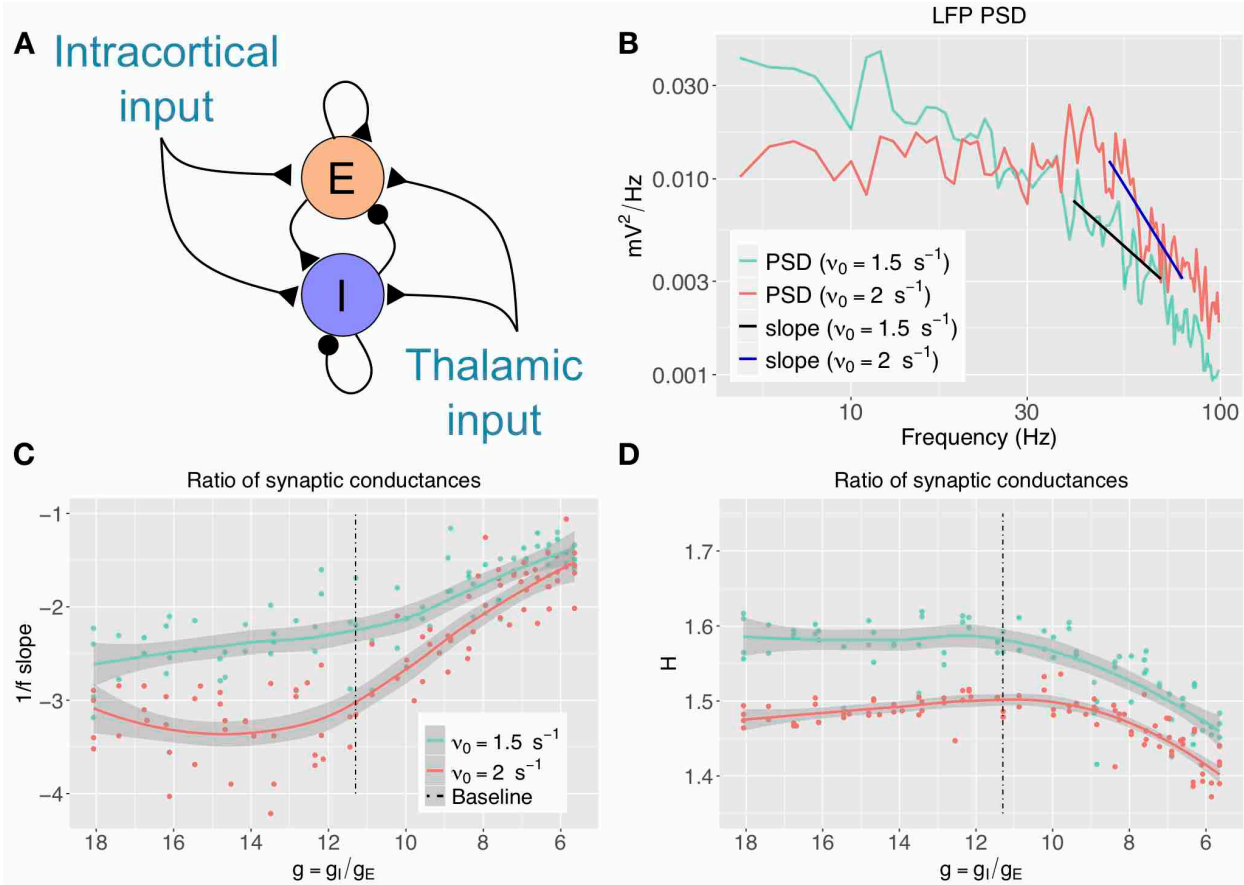

Figure 2: In-silico predictions from a recurrent network model for how 1/f slope and H behave when there are changes to the relative ratio of excitatory and inhibitory synaptic conductances. *Panel A shows a sketch of the point-neuron network that includes recurrent connections between two types of populations: excitatory cells (E) and inhibitory cells (I). Each population receives two types of external inputs: intracortical activity and thalamic stimulation. Panel B shows examples of normalized LFP power spectral densities (PSDs) generated for two different firing rates of thalamic input (υ_0=1.5 and υ_0=2 spikes/second; spikes/second indicated as s^{-1}) using the baseline reference parameters of the model. The slope of the regression line that fits the log-log plot of the LFP PSD is computed over different frequency ranges (40-70 Hz for a thalamic input of υ_0=1.5 spikes/second and 50-80 Hz for υ_0=2 spikes/second). The relationship between 1/f slope (panel C) and H (panel D) is plotted as a function of the ratio between inhibitory and excitatory conductances ($g = g_I/g_E$). The baseline reference value of parameters (which has shown in previous studies to reproduce cortical data well) is represented by a dashed black line.*

Enhancing excitability of excitatory neurons in the recurrent network model

We next investigated manipulations of candidate recurrent network model parameters that approximate the effects of empirical Designer Receptors Exclusively Activated by Designer Drugs (DREADD) manipulations of neurons. These simulations are useful to both gain a better understanding of the empirical BOLD measures under DREADD manipulations presented in the next section, and to better characterize the specificity of the origin of the 1/f slope in terms of the E:I ratio. We first studied the specific effect of solely increasing excitation within the recurrent

network model. This can be achieved experimentally by using the hM3Dq DREADD manipulation to increase the excitability of excitatory neurons only[38]. We simulated this manipulation by increasing the excitability of pyramidal neurons in the recurrent network model by lowering their voltage threshold (V_{th}) for spike initiation. In the range in which excitation is increased with respect to the baseline reference parameter, -52 to -53 mV, the 1/f slopes were flatter and H decreased (Figure 3A). When V_{th} increased from the baseline reference value, we observed no detectable changes in 1/f slope or H. Similar results were found with an alternative, yet similarly realistic manipulation in which we applied an external constant small current (I_e) to pyramidal neurons (see Supplementary Figure 1A-B). These results predict that specific increases of excitation, as in the application of the hM3Dq DREADD to enhance excitability of pyramidal neurons, should flatten the 1/f slope and lead to a decrease in H. These results also confirm our above finding that, in recurrent networks in which excitatory and inhibitory neurons interact, decreases in excitation from a baseline reference value are harder to detect from 1/f slopes or H than increases in excitation.

Silencing both excitatory and inhibitory neurons in the recurrent network model

To study whether the changes in 1/f slope are specific to modulations in excitability of only excitatory neurons, we modeled the effect of an overall change in excitability of both excitatory and inhibitory neurons. A decrease in excitability of both excitatory and inhibitory neurons can be obtained experimentally by application of the hM4Di DREADD under the control of a pan-neuronal promoter (see next Section). In the recurrent network model, we simulated a reduction of overall excitability of excitatory and inhibitory cells by decreasing the resting potential, E_L, in both excitatory and inhibitory neurons. Decreasing E_L from the baseline reference value of -70 to -75 mV produced flatter 1/f slopes for υ_0 = 2 spikes/second (1/f slope for υ_0 = 1.5 spikes/second remained largely unaltered), and resulted in a slight increase of H (Figure 3B). However, these effects were far less prominent than those observed when enhancing excitation specifically (Figure 3A). Similar results were found when modelling the possible effect of the hM4Di DREADD as a silencing of the network through an overall reduction of the transmission probability of recurrent synapses ($p_{transmit}$) (Supplementary Figure 1C-D). Given that BOLD dynamics are less sensitive to changes in 1/f slope and H than the underlying neural dynamics (Figure 1D), these results predict a very small, or null, effect of the hM4Di DREADD on BOLD H and 1/f slope. These results also imply that decreased H in BOLD signal are more likely to result from specific increases in excitation than from non-specific decreases of excitability across both excitatory and inhibitory neuronal populations.

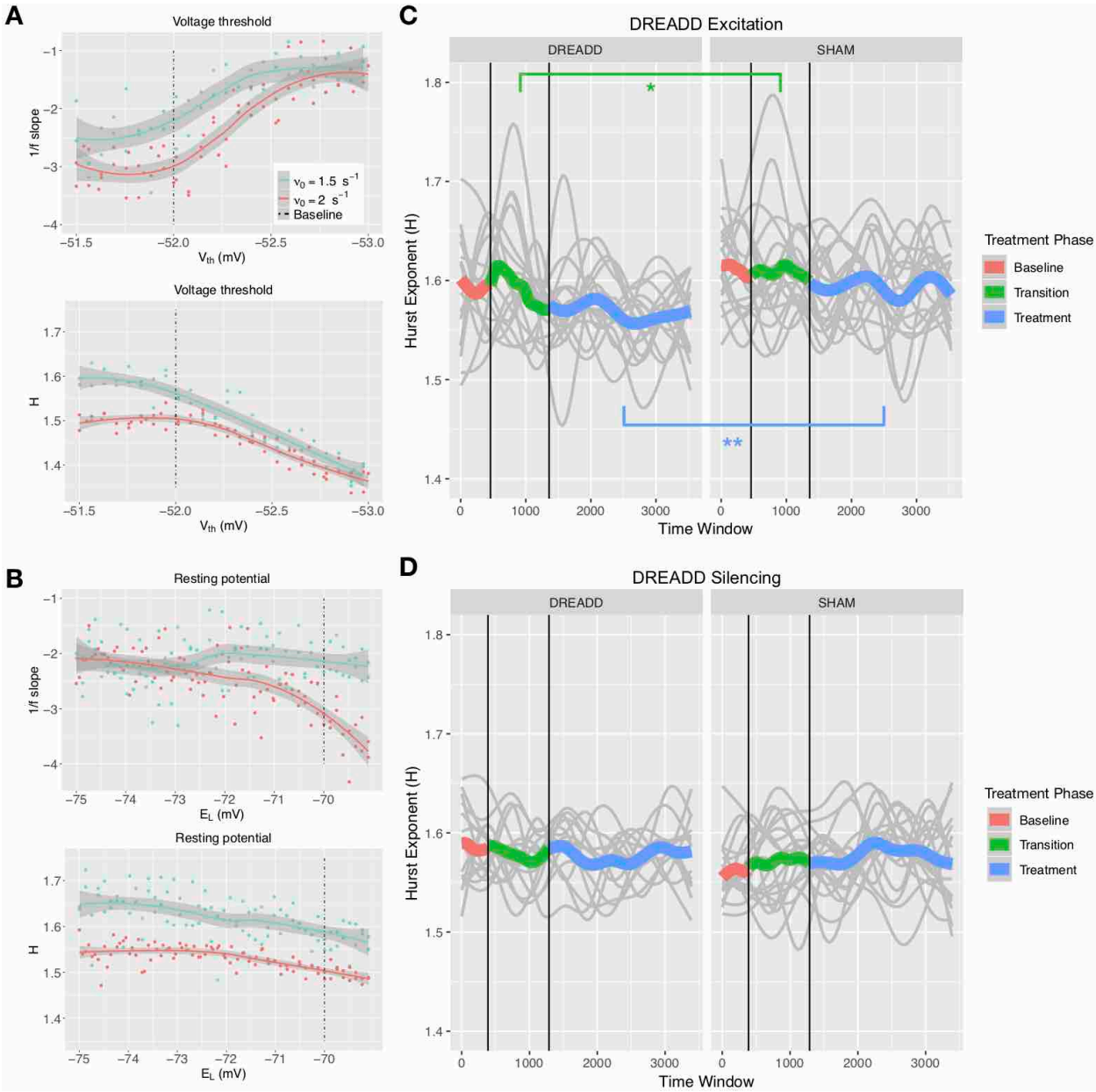

Figure 3: Effect of manipulations to enhance excitation of excitatory neurons or to silence excitatory and inhibitory neurons. *Panel A shows how 1/f slope and H behave in a manipulation of the recurrent network model to simulate the effects of enhanced excitation of excitatory neurons that recapitulates the experimental manipulation of hM3Dq DREADD. This manipulation enhances excitability of excitatory neurons by varying the voltage threshold for spike initiation in excitatory neurons* (V_{th}) *from the baseline reference value of -52 mV to -53 mV. Panel B shows how 1/f slope and H behave under a manipulation of the recurrent network model to simulate the effects of silencing both excitatory and inhibitory neurons that recapitulates the experimental manipulation of hM4Di DREADD. This manipulation varies the resting potential of excitatory and inhibitory neurons* (E_L) *from the baseline reference value of -70 mV to -75 mV. Baseline reference values are indicated as the dashed line in panels A and B. Turquoise and pink lines in panels A and B represent data for two different firing rates of thalamic input (*υ_0*=1.5 (turquoise) and* υ_0*=2 spikes/second (pink)). Panel C shows the hM3Dq DREADD manipulation to enhance excitability*

*of excitatory neurons, while panel D shows the hM4Di DREADD manipulation to silence activity in both excitatory and inhibitory neurons. Baseline (pink), transition (green), and treatment (blue) periods are annotated with different colors. Data from each individual mouse is shown in light gray. * = p<0.05, ** = p < 0.005.*

Changes in H in BOLD after chemogenetic manipulation to enhance excitability of excitatory neurons

The *in-silico* modeling presented thus far makes the prediction that in real BOLD data, if E:I ratio is increased via enhanced excitability of excitatory neurons, then H should decrease. To empirically test this prediction, we measured rsfMRI BOLD signal in prefrontal cortex of mice under conditions where a chemogenetic manipulation (hM3Dq DREADD)[38] is used to enhance excitability of pyramidal neurons. Using a sliding window analysis, we find that H is modulated over time by the DREADD manipulation (condition*time*treatment phase interaction $F = 349.03$, $p < 0.0001$). During the baseline phase of rsfMRI scanning before the DREADD-actuator clozapine N-oxide (CNO) was injected, H under DREADD or a SHAM control conditions are not affected (condition main effect $F = 0.82$, $p = 0.37$; condition*time interaction $F = 0.36$, $p = 0.54$). However, during the transition phase of the experiment where the CNO begins to have its effects, we find a condition*time interaction ($F = 4.94$, $p = 0.0262$), whereby H drops over time at a steeper rate during the DREADD condition compared to the SHAM condition. Finally, during the treatment phase of the experiment, where the drug exerts its maximal effect, there is a significant main effect of condition ($F = 12.92$, $p = 0.0011$) and no condition*time interaction ($F = 0.66$, $p = 0.4182$) (Figure 3C) (Table 1). This effect is explained by H being reduced in the DREADD vs SHAM condition. These *in-vivo* results are directly in line with the *in-silico* prediction that enhancing the excitability of excitatory neurons results in a decrease in H as measured in real BOLD rsfMRI data.

Chemogenetically silencing both excitatory and inhibitory neurons has no effect on H in BOLD

While the above results show that specific enhancement of excitability in excitatory neurons results in a decrease in BOLD H, it is interesting to investigate whether reducing non-specifically both the excitability of excitatory and inhibitory neurons might have the opposite effect and increase H in BOLD. By expressing the inhibitory hM4Di DREADD[39] under the control of a pan-neuronal promoter, we chemogenetically reduced the excitability of both excitatory and inhibitory neurons and re-ran the same rsfMRI neuroimaging protocol as before. While a significant 3-way interaction between condition, time, and treatment phase was present ($F = 85.8$, $p < 0.0001$), there were no strong main effects of condition or condition*time interactions in any of the baseline, transition, or treatment phases of the experiment (see Table 2) (Figure 3D). Overall, these results provide some specificity for the effects of enhanced excitation as the primary driver behind decreasing H in BOLD. Non-specific silencing of activity has no remarkable reverse effects of increasing H in BOLD. These *in-vivo* results are again in line with *in-silico* predictions and directly showcase that *in-silico* predictions derived from simulated LFP data translate to empirical differences in H in BOLD data.

H is on-average reduced in adult autistic men but not women

Having demonstrated *in-silico* and *in-vivo* that enhanced excitation reduces H in LFP and rsfMRI BOLD data, we move to application of this work to human rsfMRI data in adult autistic men and women. If E:I ratio is affected by sex-related mechanisms[13], we predict that H would be differentially affected in autistic males versus females and manifest as sex-by-diagnosis interactions in a 2x2 factorial design (Sex: Male vs Female; Diagnosis: Autism vs Typically-Developing (TD)). Mass-univariate analysis uncovered one region in ventromedial prefrontal cortex (vMPFC) with a sex-by-diagnosis interaction passing FDR q<0.05 ($F(5,104) = 15.13$, $p = 0.0001$, *partial* $\eta^2 = 0.12$) (Figure 4A). This interaction effect is driven by a large TD>Autism effect in males (*Cohen's d* = 1.30) and a small Autism>TD effect in females (*Cohen's d* = -0.27) (Figure 4B). We also used a multivariate partial least squares (PLS) analysis to uncover that vMPFC is part of a more distributed neural system expressing the same sex-by-diagnosis interaction ($d = 2.04$, $p = 0.036$) as other areas that include relevant default mode network (DMN) areas in posterior cingulate cortex/precuneus (PCC) (Supplementary Figure 2), and other non-DMN areas such as insula, lateral prefrontal cortex, somatosensory and motor cortices, amongst others (Figure 4C). The PLS result allows for detection of other regions that were subthreshold in the mass-univariate analysis, but which showed heightened effect sizes (e.g., white and light blue areas in the unthresholded map shown in Figure 4A). Detection of these regions in a mass-univariate analysis may require a larger sample size to enhance statistical power.

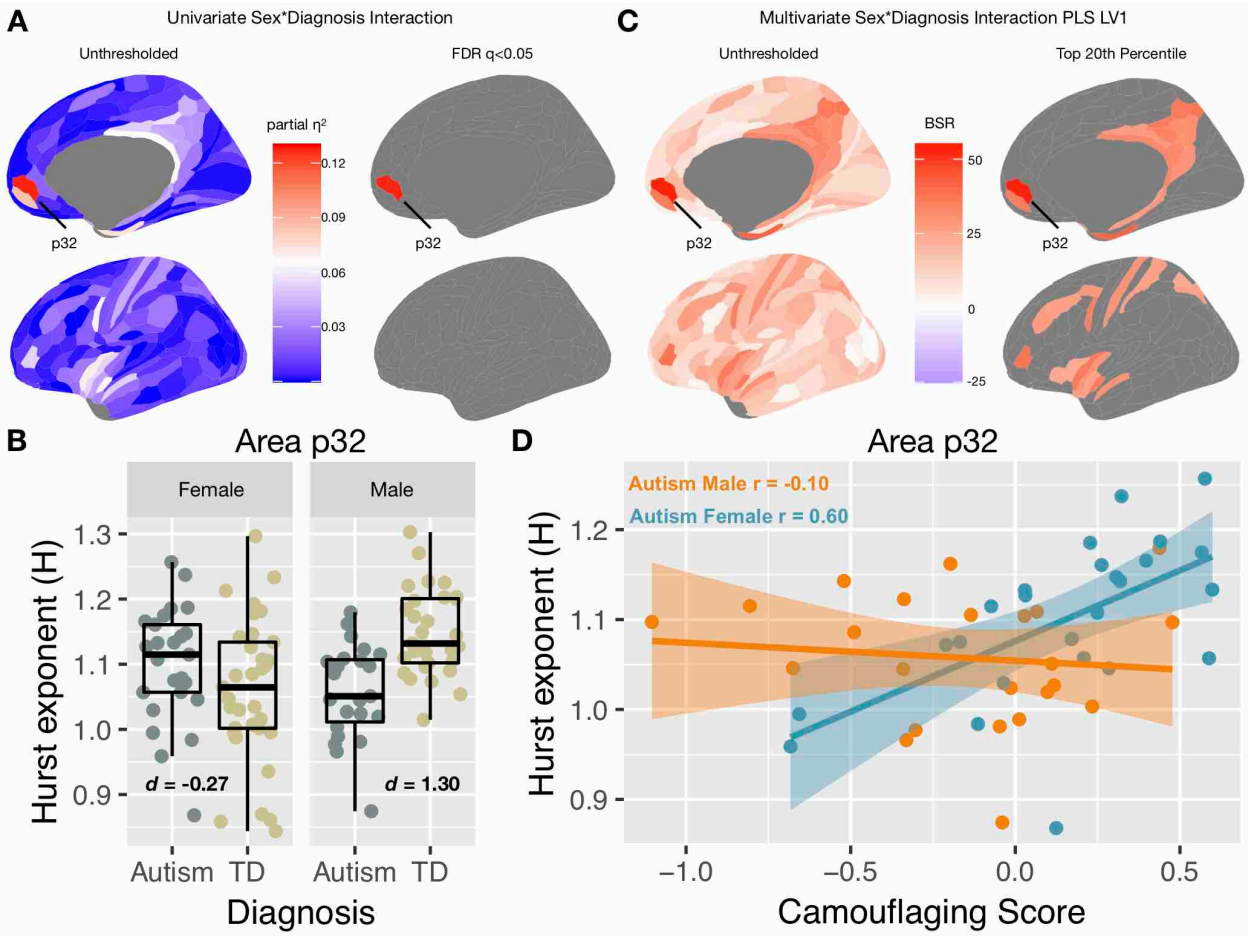

Figure 4: Autism rsfMRI results. *Panel A shows unthresholded and thresholded with FDR q<0.05 mass-univariate results for the sex*diagnosis interaction contrast. Panel B shows H estimates from vMPFC (area p32) across males and females with and without autism. Panel C shows partial least squares (PLS) results unthresholded and theresholded to show the top 20% of brain regions ranked by bootstrap ratio (BSR). Panel D shows correlation between vMPFC H and behavioral camouflaging score in autistic males (orange) and females (blue).*

Correlation between H and camouflaging in autistic women but not men

In prior task-evoked fMRI work we found a similar sex-by-diagnosis interaction in vMPFC self-representation response and a female-specific brain-behavioral correlation with camouflaging ability[19]. Given that adult autistic females engage more in camouflaging on-average[16–18], we next tested the hypothesis of whether H as an index of intrinsic E:I balance, would be related to camouflaging in a sex-specific manner. In autistic females, increased camouflaging was strongly associated with increased H in vMPFC (r = 0.60, p = 0.001). However, no significant association was apparent in autistic males (r = -0.10, p = 0.63). The strength of this brain-behavioral correlation significantly differed between autistic males and females (z = 2.58, p = 0.009) (Figure 4D).

Discussion

In this work we set out to better understand how intrinsic E:I imbalance affects the autistic brain. Evidence from animal models of rare genetic variants associated with autism have typically been used as the primary evidence for the E:I imbalance theory[1,2]. However, these variants affect only a small percentage of the autism population. Thus, it is unclear how E:I imbalance might affect the majority of heterogeneous individuals within the total autism population. To bridge this gap we need multi-level methods that can be applied to understand the 'living biology' behind actual human individuals[40], such as in-vivo neuroimaging data and metrics applied to such time-series data that are linked to actual underlying neural E:I mechanisms. Bridging this gap will help us identify mechanistic targets that explain neural and behavioral variability across a much larger portion of individuals in the autism population.

Based on earlier computational models of E:I imbalance[24], we reasoned that metrics of scale-free signal complexity characterizing asynchronous 1/f background signal of neural time-series data would be relevant as an *in-vivo* neuroimaging marker of E:I mechanisms. Prior work[24] suggested this relationship via a model that considers inhibition and excitation as separate entities. However, excitation and inhibition in the brain are inseparably linked. Furthermore, prior work[24] considered only 1/f slopes in simulated LFP data and did not explore the effect of the transformation between LFP neural activity to BOLD. Our simulations address these problems and significantly extend prior work[24] on the relationship between E:I imbalance and 1/f slope. We showed that when excitation and inhibition interact in a recurrent network model, flatter 1/f slopes and decreases in H are specific markers of increases in E:I ratio. We showed that H tracks with the 1/f slope, with decreases in H corresponding to flatter 1/f slopes. We showed that convolution of neural signals with the HRF leads to flattening of the relationship between 1/f signal and H. Taken together, these results imply that changes in H found in fMRI BOLD data can be interpreted as a

shift in E:I balance in the underlying LFP data that is proportionally larger than the change in H observed BOLD.

The power of our *in-silico* modeling approach is that it provides explicit predictions of what to expect in real BOLD data when E:I imbalance occurs in the underlying neural data. Remarkably, these *in-silico* predictions are confirmed *in-vivo* with rsfMRI BOLD data in mice after experimental chemogenetic manipulations that specifically enhance neural excitation. Intriguingly, and consistent with *in-silico* predictions, non-specific manipulations that decrease the excitability of both excitatory and inhibitory neurons do not have a detectable effect on H in BOLD. These results are in line with optogenetic studies showing that specifically enhancing excitation in MPFC seems to have the biggest effects on social behavior in mice[14]. The present work clearly shows that enhancement of neurophysiological excitation results in measurable changes in BOLD readouts as decreases in H levels. This insight allows us to leverage H as an *in-vivo* biomarker in rsfMRI data that has strong relevance back to E:I neurophysiological mechanisms.

In human rsfMRI data we utilized H as a neuroimaging biomarker of E:I imbalance. Specifically, we examined whether H differs between adult males and females with and without autism. Mass-univariate analysis highlighted one region, vMPFC, which showed a sex-by-diagnosis interaction - that is, H was specifically reduced in adult autistic males, but not in autistic females. Reduced H in autistic males is compatible with the inference of elevated E:I ratio potentially driven by enhanced excitation. Multivariate PLS analysis extended this finding by showing that a distributed neural system structurally and functionally connected to vMPFC, such as default mode network (DMN) areas like PCC[41,42], also expressed a similar but more subtle sex-by-diagnosis interaction. Therefore, important social brain circuitry such as the DMN, may be asymmetrically affected by heightened E:I ratio in autistic males more than autistic females. These results are not only compatible with the *in-silico* predictions and the *in-vivo* mouse rsfMRI data presented here, but is also compatible with several prior lines of work. Our prior work highlighted that DMN functional connectivity in adolescent males, but not females, is affected by heightened levels of fetal testosterone and this network was heavily comprised of MPFC and PCC[13]. In the same work, we showed that a cortical midline DMN subsystem comprising MPFC and PCC highly expresses several genes relevant for excitatory postsynaptic potentials (e.g., *MEF2C, GRIK2, GRIA1, SCN3A, SCN9A, NPTX2*). Importantly, the expression of these genes in human neuronal stem cells are elevated after exposure to the potent androgen DHT[13]. Thus, one potential explanation for the male-specific reduction of H in vMPFC could have to do with early developmental and androgen-sensitive upregulation of genes that play central roles in excitatory postsynaptic potentials, and thus ultimately affecting downstream E:I imbalance. Such effects may be sex-differential and thus less critical in human females, serving an important basis of sex-differential human brain development[43] and explaining the sex-based heterogeneity and qualitative sex differences of autism neurobiology in human[10,44].

rsfMRI H in autistic adults was also relevant in a sex-specific manner to a clinical behavioral phenomenon known as 'camouflaging'. Camouflaging relates to a set of compensatory or masking strategies or mechanisms that allows individuals to cope with their social-communicative difficulties in everyday social situations[16,17,45]. It is known that cognitively able adult autistic females tend to engage in more camouflaging behavior than males[16–18] and the extent

to which individual females engage in camouflaging is linked to vMPFC function[19]. One of the most important known functions of vMPFC has to do with self-representation[46] and simulating others based on information about the self[47]. In prior task-evoked fMRI work we found a similar sex-by-diagnosis interaction effect whereby males are more impaired in vMPFC self-representation response than their female autistic counterparts. Furthermore, increased magnitude of vMPFC self-representation neural response correlates with increased camouflaging ability, but only in adult autistic females[19]. Strikingly, here we find a similar sex-by-diagnosis interaction effect in vMPFC H as well as a female-specific correlation with camouflaging - as vMPFC H increases, indicative of a more normative or intact level of E:I balance, camouflaging also increases. This converging set of results provides strong evidence that intrinsic mechanisms such as E:I balance may be atypical only in cognitively able autistic males at vMPFC. vMPFC in similarly cognitively able autistic females likely has more intact, or normalized, intrinsic E:I balance and this more intact mechanism potentially allows for intact levels of neural self-representation and enhanced camouflaging ability. Future work changing E:I balance in vMPFC may provide a useful avenue for ameliorating daily life social-communication adaptation and coping difficulties in autistic males and enable them to optimally engage in compensatory processes such as camouflaging to the similar extent as autistic females, despite the underlying potentially sex-differential neurobiological bases of autism. It may also be fruitful to examine how intact E:I balance in vMPFC of females may be an expression of protective factors that are hypothesized to buffer risk for autism in females[48,49].

In conclusion, we show that scale-free metrics from *in-vivo* neuroimaging data in humans such as H can be utilized as a biomarker for underlying E:I-relevant mechanisms. *In-silico* predictions from simulated LFP and BOLD data were confirmed *in-vivo* with rsfMRI BOLD data where excitation was enhanced through chemogenetic manipulation. Finally, in application to humans, we show that H in rsfMRI data is reduced in vMPFC and other DMN areas of adult autistic males, but not females. Reduced H is indicative of enhanced excitation and thus points to sex-specific dysregulation of E:I balance in social brain networks of autistic males. This male-specific dysregulation of E:I balance may be linked to sex-differential early developmental events such as androgen-upregulation of gene expression for genes that play important roles in excitatory postsynaptic potentials[13]. The intact levels of H in females may help facilitate elevated levels of compensation known as camouflaging to cope with daily social-communicative difficulties. This important female-specific brain-behavioral correlation may also be key for future innovation in intervention targeting E:I mechanisms and MPFC-related brain regions that may enable better coping with daily social-communicative adaptation difficulties related to autism. More generally, this work extends the relevance of the E:I imbalance theory of autism beyond evidence from autism-associated rare genetic variants and specify a larger portion of the autism population whereby these E:I mechanisms may be of critical importance.

Methods

Human Participants

All procedures contributing to this work comply with the ethical standards of the relevant national and institutional committees on human experimentation and with the Helsinki Declaration of 1975, as revised in 2008. All human participants' informed consent was obtained in accord with procedures approved by the Suffolk Local Research Ethics Committee. Adult native English speakers (n=136) with normal/corrected-to-normal vision participated: n=33 typically developing (TD) males, n=34 autistic males, n=34 TD females and n=34 autistic females (Table 3). They all reported cis-gender identity based on a single item inquiring their birth-assigned sex and another on their identified gender. Groups were not statistically different on age or full-scale IQ (FIQ) on the Wechsler Abbreviated Scales of Intelligence (WASI) (Table 3). Exclusion criteria for all participants included a history of or current psychotic disorders, substance-use disorders, severe head injury, genetic disorders associated with autism (e.g. fragile X syndrome and tuberous sclerosis), intellectual disability (i.e. Full-scale IQ (FIQ) < 70), or other medical conditions significantly affecting brain function (e.g. epilepsy).

The inclusion criterion for both male and female autistic participants was a formal clinical diagnosis of International Statistical Classification of Diseases and Related Health Problems 10th Revision (ICD-10) childhood autism or Asperger's syndrome, or Diagnostic and Statistical Manual of Mental Disorders (4th ed., text rev.; DSM-IV-TR) autistic disorder or Asperger's disorder, as assessed by a psychiatrist or clinical psychologist in the National Health Service, UK. Since all participants were adults, we further considered available information of developmental history to include only those with clinically evident childhood autistic symptoms, for example, from information collected using the Autism Diagnostic Interview–Revised (ADI-R)[50] where possible, or from the participants' clinical diagnosis letters shared with the research team to determine eligibility. We used this clinically based criterion for inclusion for the purpose of sampling autistic individuals currently diagnosed by specialists in mental health services in the daily practice and to align with best clinical practice as recommended by the UK National Institute for Health and Clinical Excellence (NICE) guideline (Pilling et al., 2012). For assessing levels of autism characteristics, we administered the Autism Spectrum Quotient (AQ)[51], module 4 of the Autism Diagnostic Observation Schedule (ADOS)[52], and ADI-R[50] where possible, before the fMRI session. Autistic male and female groups were not different on ADI-R Reciprocal-Social-Interaction scores or Reading the Mind in the Eyes Test (RMET)[53] performance (Table 3).

We further used criteria for inclusion based on characteristics about data quality (see next paragraphs for data preprocessing). In particular, we excluded participants where the number of volumes was not acquired due to scanner hardware issues (n=1), the preprocessing pipeline could not adequately preprocess the data (e.g., bad registrations; n=5). Participants were also excluded if their head motion exceed a mean framewise displacement (meanFD) of >0.4mm (n=8). For the remaining subjects we further visually inspected plots of framewise displacement (FD) and DVARS[54] traces to determine whether the wavelet despiking step sufficiently attenuated artefact-related variability that would leave DVARS spikes (see below Human fMRI data analysis). Here we made a qualitative and consensus judgement amongst authors (S.T. and M.V.L) to exclude

individuals (n=9) whereby there were numerous FD spikes above 0.5mm or numerous DVARS spikes leftover after wavelet despiking was applied. Other exclusions included any VIQ or PIQ <70 (n=1) and co-morbid agenesis of the corpus callosum (n=1). The final sample sizes included in all further analyses was n=29 TD males, n=23 autistic males, n=33 TD females, and n=25 autistic females. The final groups used in all analyses did not statistically differ on age (Diagnosis main effect: $F(3,106) = 0.03$, $p = 0.85$; Sex main effect: $F(3,106) = 0.14$, $p = 0.70$; Sex*Diagnosis interaction: $F(3,106) = 0.25$, $p = 0.61$) or FIQ (Diagnosis main effect: $F(3,106) = 3.38$, $p = 0.07$; Sex main effect: $F(3,106) = 0.48$, $p = 0.48$; Sex*Diagnosis interaction: $F(3,106) = 2.24$, $p = 0.13$) (see Table 3).

Human fMRI data acquisition

Imaging was performed on a 3T GE Signa Scanner at the Cambridge Magnetic Resonance Imaging and Spectroscopy Unit. Participants were asked to lie quietly in the scanner awake with eyes closed for 13 minutes and 39 seconds during sequential acquisition of 625 whole-brain T2*-weighted echo planar image volumes with the following parameters: relaxation time = 1302 msec; echo time = 30 msec; flip angle = 70°; matrix size = 64 x 64; field of view = 24 cm; 22 anterior commissure-posterior commissure aligned slices per image volume; 4 mm axial slice thickness; 1 mm slice gap. The first five time-points were discarded to allow for T2-stabilization. During analysis of the Hurst exponent (H) for BOLD time-series, due to the discrete wavelet transform using volumes in power of 2, only the first 512 volumes (2^9) were utilized. A high-resolution spoiled gradient anatomical image was acquired for each participant for registration purposes.

Human fMRI data analysis

Preprocessing of the resting state data was split into two components; core preprocessing and denoising. Core preprocessing was implemented with AFNI[55] (http://afni.nimh.nih.gov/) using the tool speedypp.py (http://bit.ly/23u2vZp)[56]. This core preprocessing pipeline included the following steps: (i) slice acquisition correction using heptic (7th order) Lagrange polynomial interpolation; (ii) rigid-body head movement correction to the first frame of data, using quintic (5th order) polynomial interpolation to estimate the realignment parameters (3 displacements and 3 rotations); (iii) obliquity transform to the structural image; (iv) affine co-registration to the skull-stripped structural image using a gray matter mask; (v) nonlinear warping to MNI space (MNI152 template) with AFNI 3dQwarp; (v) spatial smoothing (6 mm FWHM); and (vi) a within-run intensity normalization to a whole-brain median of 1000. Core preprocessing was followed by denoising steps to further remove motion-related and other artifacts. Denoising steps included: (vii) wavelet time series despiking ('wavelet denoising'); (viii) confound signal regression including the 6 motion parameters estimated in (ii), their first order temporal derivatives, and ventricular cerebrospinal fluid (CSF) signal (referred to as 13-parameter regression). The wavelet denoising method has been shown to mitigate substantial spatial and temporal heterogeneity in motion-related artifact that manifests linearly or non-linearly and can do so without the need for data scrubbing[57]. Data scrubbing (i.e. volume censoring) cannot be used in our time-series-based analyses here as such a procedure breaks up the temporal structure of the time-series in such a way that invalidates estimation of the Hurst exponent (H) that examine long-memory characteristics. Wavelet denoising is implemented with the Brain Wavelet toolbox (http://www.brainwavelet.org). The 13-parameter regression of motion and CSF signals was achieved using AFNI 3dBandpass

with the –ort argument. To further characterize motion and its impact on the data, we computed FD and DVARS[54]. Between-group comparisons showed that all groups were similar with respect to head motion as measured by meanFD with no Diagnosis ($F(3,106) = 1.77$, $p = 0.18$) or Sex ($F(3,106) = 0.51$, $p = 0.47$) main effects or Sex*Diagnosis interaction ($F(3,106) = 1.10$, $p = 0.29$). All groups showed average meanFD of less than 0.2 mm (see Table 3).

Mean time-series for each of the 180 parcels within the Human Connectome Project Multimodal Parcellation (HCP-MMP)[58] were extracted from the final preprocessed data, to estimate H. The estimation of H utilizes a discrete wavelet transform and a model of the time-series as fractionally integrated processes (FIP) and is estimated using maximum likelihood estimation. This method utilizing the FIP model for estimating H differs from our prior work[23], which used a model of fractional Gaussian noise (fGn). fGn is one type of process subsumed under the FIP model. However, the fGn model has the limitation of assuming that the BOLD time-series is stationary and also limits the upper bound of H at 1. In practice, we have seen that the upper bound of H=1 from the fGn model results in ceiling effects for many brain regions and subjects. Thus, to remove the assumption of stationarity and upper bound of H=1, the FIP model offers more flexibility and potentially added sensitivity due to better estimation of between-subject variability when estimates are near or exceed H=1. When H>1 the time-series is considered non-stationary and has long memory characteristics (e.g., is fractal). H is computed using the nonfractal MATLAB toolbox written by one of the co-authors (WY) (https://github.com/wonsang/nonfractal). The specific function utilized is bfn_mfin_ml.m function with the 'filter' argument set to 'haar' and the 'ub' and 'lb' arguments set to [1.5,10] and [-0.5,0], respectively.

After H was estimated for each of the 180 HCP-MMP parcels, we used a general linear model to test for Sex*Diagnosis interactions as well as main effects of Sex and Diagnosis in H. These models also incorporated meanFD and FIQ as covariates of no interest. Multiple comparison correction was achieved using an FDR q<0.05 threshold. Visualization of effect sizes for figures was achieved using the ggseg library in R (https://github.com/LCBC-UiO/ggseg).

In addition to mass-univariate analysis, we also utilized multivariate partial least squares (PLS) analysis[59] to highlight distributed neural systems that capture the effect of a sex*diagnosis interaction. This analysis was implemented with code from the plsgui MATLAB toolbox (http://www.rotman-baycrest.on.ca/pls/). A matrix with participants along the rows and all 180 HCP-MMP parcels along with columns was input as the primary neuroimaging matrix for PLS. We also inserted a vector describing the sex*diagnosis contrast as the matrix to relate to the neuroimaging matrix. This vector describing the sex*diagnosis interaction was computed by matrix multiplication of the contrast vector of [1, -1, -1, 1] to a design matrix that was set up with columns defining TD males, autism males, TD females, and autism females, respectively. The PLS analysis was run with 10,000 permutations to compute p-values for each latent-variable (LV) pair and 10,000 bootstrap resamples in order to compute bootstrap ratios (BSR) to identify brain regions of importance for each LV pair. To isolate specific brain regions of importance for a statistically significant LV, we selected the top 20th percentile of brain regions ranked by BSR.

Relationships between H and camouflaging were conducted within autistic males and females separately. Pearson's correlations were used to estimate the strength of the relationship

and groups were compared on the strength of the relationship using Fisher's r-to-z transform as implemented with the paired.r function in the *psych* library in R.

Behavioral index of camouflaging

Camouflaging (consciously or unconsciously compensating for and/or masking difficulties in social–interpersonal situations) was operationalized as prior work[16,19]: the discrepancy between extrinsic behavioral presentation in social–interpersonal contexts and the person's intrinsic status. We used both the AQ score and RMET correct score as reflecting intrinsic status (i.e. self-rated dispositional traits and performance-based socio-cognitive/mentalizing capability), and the ADOS Social-Communication total score as reflecting extrinsic behavioral presentation. The three scores were first standardized (S_{ADOS}, S_{AQ} and S_{RMET}) within our sample of autistic men and women by mean-centring (to the whole autism sample in this study) and scaling (i.e. divided by the maximum possible score of each) to generate uniformly scaled measures that can be arithmetically manipulated. The first estimate of camouflaging was quantified as the difference between self-rated autistic traits and extrinsic behaviors ($CF1 = S_{AQ} - S_{ADOS}$), and the second estimate between mentalizing ability and extrinsic behaviors ($CF2 = -S_{RMET} - S_{ADOS}$). Then, using principal component analysis, the first principal component score of CF1 and CF2 (accounting for 86% of the total variance) was taken as a single, parsimonious measure of camouflaging for all subsequent analyses. This measure should be interpreted by relative values (i.e. higher scores indicate more camouflaging) rather than absolute values. This operationalization only allows for estimating camouflaging in autistic individuals in our cohort, as it partly derives from the ADOS score which was not available in TD participants. This approach remains informative, as qualitative studies suggest that camouflaging in autism can be different from similar phenomenon (e.g. impression management) in TD individuals[60,61].

In-vivo chemogenetic manipulation of excitation in mouse prefrontal cortex

All *in-vivo* studies in mice were conducted in accordance with the Italian law (DL 116, 1992 Ministero della Sanità, Roma) and the recommendations in the Guide for the Care and Use of Laboratory Animals of the National Institutes of Health. Animal research protocols were also reviewed and consented to by the animal care committee of the Istituto Italiano di Tecnologia. The Italian Ministry of Health specifically approved the protocol of this study, authorization no. 852/17 to A.G. All surgical procedures were performed under anesthesia.

Six to eight week-old adult male C57Bl6/J mice (Jackson Laboratories; Bar Harbor, ME, USA) were anesthetized with isoflurane (isofluorane 4%,) and head-fixed in a mouse stereotaxic apparatus (isofluorane 2%, Stoelting). Viral injections were performed with a Hamilton syringe mounted on Nanoliter Syringe Pump with controller (KD Scientific), at a speed of 0.05 μl/min, followed by a 5–10 min waiting period, to avoid backflow of viral solution and unspecific labeling. Viral suspensions were injected bilaterally in PFC using the following coordinates, expressed in millimeter from bregma: 1.7 from anterior to posterior, 0.3 lateral, −1.7 deep. The inhibitory DREADD hM4Di was transduced using an AAV8-hSyn-hM4D(Gi)-mCherry construct. Control animals were injected with a control AAV8-hSyn-GFP virus (www.addgene.com). These viral suspensions were injected using a 0.3 μL injection volume in n=15 hM4Di DREADD and n=19 SHAM mice, respectively. The excitatory DREADD hM3Dq was transduced using an AAV8-

CamkII-hM3D (Gq)-mCherry construct. Control animals for this experiment were injected with a control AAV8-hSyn-GFP construct. This set of injection were carried out using a 1μL injection volume in n=17 hM3Dq DREADD and n=19 SHAM mice, respectively. We waited at least 3 weeks to allow for maximal viral expression.

Mouse rsfMRI data acquisition

The animal preparation protocol for mouse rsfMRI scanning was previously described in detail[62]. Briefly, mice were anesthetized with isoflurane (5% induction), intubated and artificially ventilated (2% maintenance). Then isoflurane was discontinued and substituted with halothane (0.75%), a sedative that preserves cerebral blood flow auto-regulation and neurovascular coupling[63]. Functional data acquisition commenced 30 min after isoflurane cessation. CNO (2 mg/kg for hM4Di and 0.5 mg/kg for hM3Dq) was administered i.v. after 15 minutes from the beginning of the acquisition both in virally transduced animals and in sham mice.

Mouse rsfMRI data analysis

Raw mouse rsfMRI data was preprocessed as described in previous work[64,65]. Briefly, the initial 120 volumes of the time series were removed to allow for T1 and gradient equilibration effects. Data were then despiked, motion corrected and spatially registered to a common reference template. Motion traces of head realignment parameters (3 translations + 3 rotations) and mean ventricular signal (corresponding to the averaged BOLD signal within a reference ventricular mask) were used as nuisance covariates and regressed out from each time course. All rsfMRI time series also underwent band-pass filtering to a frequency window of 0.01–0.1 Hz and spatial smoothing with a full width at half maximum of 0.6 mm.

The experimental design of the study allowed for computation of H during time-windows in the rsfMRI scan before drug injection (e.g., "Baseline"), a transition phase where the drug begins having its effect (e.g., "Transition"), and a treatment phase when the drug is thought to have its optimal effect (e.g., "Treatment"). Analysis of condition, treatment phase, time, and all interactions between such factors was achieved using a sliding window analysis. Each window was 512 volumes in length and the sliding step was 1 volume. H is computed at each window and results in an H time-series. The H time-series is used as the dependent variable in a linear mixed effect model (i.e. using the *lme* function within the *nlme* library in R) with fixed effects of condition, time, treatment phase, and all 2-way and 3-way interactions between such factors as well as a factor accounting for scan day. Random effects in the model included time within mouse as well as treatment phase within mouse, all modeled with random intercepts and slopes. This omnibus model was utilized to examine a 3-way interaction between condition, time, and treatment phase. If this interaction was present, we then split the data by the 3 levels of the treatment phase (e.g., Baseline, Transition, and Treatment), in order to examine the main effect of condition or the condition*time interaction. Plots of the data indicate each mouse (grey lines in Figure 3) as well as group trajectories for each phase, with all trajectories estimated with a generalized additive model smoother applied to individual mice and group trajectories.

In-silico modeling of LFP and BOLD data with a non-recurrent model

To establish that E:I ratio results in changes in H measured in LFP data in the case in which excitatory and inhibitory neurons do not interact neither across classes nor within each class, we first utilized the computational model from Gao et al.,[24]. This model simulates spike trains generated with exponential interspike intervals, and then computes the simulated LFP as a sum of excitatory and inhibitory post-synaptic AMPA and GABA currents, respectively. The higher slope of higher E;I ratio in this model arises because the AMPA currents have a faster decay and thus they have a higher power at high frequencies. Using this model, we simulated LFPs based on user-input E:I ratios spanning from 1:2 to 1:6. All other parameters in the model stay consistent with parameters used by Gao et al.,[24] (https://github.com/voytekresearch/EISlope) (see Table 4). To simulate LFP data based on manipulations to 1/f slope, we used the neurodsp library in python (https://neurodsp-tools.github.io/neurodsp/). First, we simulated 35 minutes (sampling rate = 500 Hz) of LFP data only using manipulations to 1/f slope (range 0 to -2 in steps of -0.1) and then computed H on the final LFP time-series. The final LFP time-series was also convolved with a canonical hemodynamic response function to simulate BOLD signal.

In-silico recurrent network modeling of LFP and BOLD data

To establish how E:I ratio results in changes in H measured in LFP data in the more realistic case in which excitatory and inhibitory neurons interact both across classes and within each class, we use recurrent integrate-and-fire network modelling. The network structure and parameters of the recurrent network model are the same ones used in Cavallari et al.,[30] with conductance-based synapses (for full details see[30]). In brief, the network is composed of 5000 neurons, of which 4000 are excitatory (i.e., they form AMPA-like excitatory synapses with other neurons) and 1000 inhibitory (forming GABA-like synapses). Neurons are randomly connected with a connection probability between each pair of neurons of 0.2. Both populations receive two different types of external Poisson inputs: a constant-rate thalamic input and an intracortical input generated by an Ornstein-Uhlenbeck (OU) process with zero mean. A description of the baseline reference parameters used in simulations is given in Table 5. As in the Gao et al[24] model, the LFP is computed as the sum of absolute values of AMPA and GABA postsynaptic currents on excitatory cells[26,31].

The estimate of the power spectral density (PSD) was computed using the Fast Fourier Transform with the Welch's method, dividing the data into ten overlapping segments with 50% overlap. The 1/f power-law exponent was computed as the slope of the least-squares regression line that fits the log-log plot of the PSD over a specific frequency range, 40-70 Hz for an external input of 1.5 spikes/second and 50-80 Hz for 2 spikes/second. Following previous literature[24,32,34–37], the range of frequencies for computing the slope is chosen after inspecting the frequency range at which there was a linear power-frequency dependence in the log-log plot. As in these previous studies, this frequency region was located straight after the gamma peak occurs. The ranges of frequencies that we selected for the slope calculation in the simulations are in close accordance with previous ranges used in the experimental literature of the LFP[24,32,34–37].

Data and code availability

Tidy data and analysis code are available at https://github.com/landiit/EI_hurst. Source code of the recurrent network model is available at https://github.com/pablomc88/EEG_proxy_from_network_point_neurons.

Acknowledgments

The Medical Research Council Autism Imaging Multicentre Study Consortium (MRC AIMS Consortium) is a UK collaboration between the Institute of Psychiatry, Psychology & Neuroscience (IoPPN) at King's College London, the Autism Research Centre, University of Cambridge and the Autism Research Group, University of Oxford. The Consortium members are in alphabetical order: Anthony J Bailey (Oxford), Simon Baron-Cohen (Cambridge), Patrick F Bolton (IoPPN), Edward T Bullmore (Cambridge), Sarah Carrington (Oxford), Marco Catani (IoPPN), Bhismadev Chakrabarti (Cambridge), Michael C Craig (IoPPN), Eileen M Daly (IoPPN), Sean CL Deoni (IoPPN), Christine Ecker (IoPPN), Francesca Happé (IoPPN), Julian Henty (Cambridge), Peter Jezzard (Oxford), Patrick Johnston (IoPPN), Derek K Jones (IoPPN), Meng-Chuan Lai (Cambridge), Michael V Lombardo (Cambridge), Anya Madden (IoPPN), Diane Mullins (IoPPN), Clodagh M Murphy (IoPPN), Declan GM Murphy (IoPPN), Greg Pasco (Cambridge), Amber NV Ruigrok (Cambridge), Susan A Sadek (Cambridge), Debbie Spain (IoPPN), Rose Stewart (Oxford), John Suckling (Cambridge), Sally J Wheelwright (Cambridge) and Steven C Williams (IoPPN). A.G., M.-C.L., and M.V.L. have equal senior author contributions. All authors, including the MRC AIMS Consortium, contributed to the conception and design of the study, performed the research, contributed to the collection of data, and provided critical inputs in the writing of the manuscript. S.T., P.M.-C., and M.V.L. analyzed the data. S.T., P.M.-C., M.-C.L., S.P., A.G., and M.V.L. drafted the manuscript.

Disclosures

E.T.B. is employed half-time by the University of Cambridge and half-time at GlaxoSmithKline plc (GSK); he holds stock in GSK. All other authors have no conflict of interests to declare.

Funding

The authors disclosed receipt of the following financial support for the research, authorship and/or publication of this article: The project was supported by the UK Medical Research Council (grant number: GO 400061) and European Autism Interventions – a Multicentre Study for Developing New Medications (EU-AIMS); EU-AIMS has received support from the Innovative Medicines Initiative Joint Undertaking under grant agreement no. 115300, resources of which are composed of financial contribution from the European Union's Seventh Framework Programme (FP7/2007-2013) and EFPIA companies' in-kind contribution. During the period of this work, M.-C.L. was supported by the Ontario Brain Institute via the Province of Ontario Neurodevelopmental Disorders Network (IDS-I l-02), the Slifka-Ritvo Award for Innovation in Autism Research from the International Society for Autism Research and the Alan B. Slifka Foundation, the Academic Scholars Award from the Department of Psychiatry, University of Toronto, the O'Brien Scholars Program in the Child and Youth Mental Health Collaborative at the Centre for Addiction and Mental Health (CAMH) and The Hospital for Sick Children, the Slaight Family Child and Youth Mental Health Innovation Fund from CAMH Foundation, and the Canadian Institutes of Health Research; M.V.L. was supported by a European Research Council (ERC) Starting Grant (ERC-2017-STG; AUTISMS; no. 755816); A. G. was supported by a European Research Council (ERC) Starting Grant (ERC-2018-STG; DISCONN; no. 802371), the Brain and Behavior Research

Foundation (NARSAD; Independent Investigator Grant; no. 25861), the Simons Foundation (SFARI 400101), the NIH (1R21MH116473-01A1) and by Telethon foundation; S. B.-C. was funded by the Autism Research Trust, the Wellcome Trust, the Templeton World Charitable Foundation, and the NIHR Biomedical Research Centre in Cambridge, during the period of this work. S. B.-C. also received funding from the Innovative Medicines Initiative 2 Joint Undertaking (JU) under grant agreement No 777394. The JU receives support from the European Union's Horizon 2020 research and innovation programme and EFPIA and AUTISM SPEAKS, Autistica, SFARI. S. B.-C. is also supported by the National Institute for Health Research (NIHR) Collaboration for Leadership in Applied Health Research and Care East of England at Cambridgeshire and Peterborough NHS Foundation Trust. The views expressed are those of the author(s) and not necessarily those of the NHS, NIHR or Department of Health and Social Care. SP was funded by a SFARI explorer grant (Grant no. 602849) and by the NIH Brain Initiative (Grants No. R01 NS108410 and No. U19 NS107464).

References

1. Rubenstein, J. L. R. & Merzenich, M. M. Model of autism: increased ratio of excitation/inhibition in key neural systems. *Genes Brain Behav.* **2**, 255–267 (2003).
2. Sohal, V. S. & Rubenstein, J. L. R. Excitation-inhibition balance as a framework for investigating mechanisms in neuropsychiatric disorders. *Mol. Psychiatry* **24**, 1248–1257 (2019).
3. Nelson, S. B. & Valakh, V. Excitatory/Inhibitory Balance and Circuit Homeostasis in Autism Spectrum Disorders. *Neuron* **87**, 684–698 (2015).
4. Happé, F., Ronald, A. & Plomin, R. Time to give up on a single explanation for autism. *Nat. Neurosci.* **9**, 1218–1220 (2006).
5. Lombardo, M. V., Lai, M.-C. & Baron-Cohen, S. Big data approaches to decomposing heterogeneity across the autism spectrum. *Mol. Psychiatry* **24**, 1435–1450 (2019).
6. Lombardo, M. V. *et al.* Different functional neural substrates for good and poor language outcome in autism. *Neuron* **86**, 567–577 (2015).
7. Lombardo, M. V. *et al.* Large-scale associations between the leukocyte transcriptome and BOLD responses to speech differ in autism early language outcome subtypes. *Nat. Neurosci.* **21**, 1680–1688 (2018).
8. Lombardo, M. V. *et al.* Default mode-visual network hypoconnectivity in an autism subtype with pronounced social visual engagement difficulties. *Elife* **8**, (2019).
9. Lai, M.-C., Lombardo, M. V., Auyeung, B., Chakrabarti, B. & Baron-Cohen, S. Sex/gender differences and autism: setting the scene for future research. *J Am Acad Child Adolesc Psychiatry* **54**, 11–24 (2015).
10. Lai, M.-C. *et al.* Imaging sex/gender and autism in the brain: Etiological implications. *J. Neurosci. Res.* **95**, 380–397 (2017).
11. Lee, E., Lee, J. & Kim, E. Excitation/Inhibition Imbalance in Animal Models of Autism Spectrum Disorders. *Biol. Psychiatry* **81**, 838–847 (2017).
12. Bozzi, Y., Provenzano, G. & Casarosa, S. Neurobiological bases of autism-epilepsy comorbidity: a focus on excitation/inhibition imbalance. *Eur. J. Neurosci.* **47**, 534–548 (2018).
13. Lombardo, M. V. *et al.* Sex-specific impact of prenatal androgens on social brain default mode subsystems. *Mol. Psychiatry* (2018) doi:10.1038/s41380-018-0198-y.
14. Yizhar, O. *et al.* Neocortical excitation/inhibition balance in information processing and social dysfunction. *Nature* **477**, 171–178 (2011).
15. Selimbeyoglu, A. *et al.* Modulation of prefrontal cortex excitation/inhibition balance rescues social behavior in CNTNAP2-deficient mice. *Sci Transl Med* **9**, (2017).
16. Lai, M.-C. *et al.* Quantifying and exploring camouflaging in men and women with autism. *Autism* **21**, 690–702 (2017).
17. Hull, L. *et al.* Gender differences in self-reported camouflaging in autistic and non-autistic adults. *Autism* 1362361319864804 (2019) doi:10.1177/1362361319864804.
18. Schuck, R. K., Flores, R. E. & Fung, L. K. Brief Report: Sex/Gender Differences in Symptomology and Camouflaging in Adults with Autism Spectrum Disorder. *J Autism Dev Disord* **49**, 2597–2604 (2019).
19. Lai, M.-C. *et al.* Neural self-representation in autistic women and association with 'compensatory camouflaging'. *Autism* **23**, 1210–1223 (2019).

20. Bullmore, E. *et al.* Colored noise and computational inference in neurophysiological (fMRI) time series analysis: Resampling methods in time and wavelet domains. *Human Brain Mapping* **12**, 61–78 (2001).
21. Maxim, V. *et al.* Fractional Gaussian noise, functional MRI and Alzheimer's disease. *Neuroimage* **25**, 141–158 (2005).
22. He, B. J. Scale-free properties of the functional magnetic resonance imaging signal during rest and task. *J. Neurosci.* **31**, 13786–13795 (2011).
23. Lai, M.-C. *et al.* A shift to randomness of brain oscillations in people with autism. *Biol. Psychiatry* **68**, 1092–1099 (2010).
24. Gao, R., Peterson, E. J. & Voytek, B. Inferring synaptic excitation/inhibition balance from field potentials. *Neuroimage* **158**, 70–78 (2017).
25. Stadnitski, T. Measuring fractality. *Front Physiol* **3**, 127 (2012).
26. Mazzoni, A., Panzeri, S., Logothetis, N. K. & Brunel, N. Encoding of naturalistic stimuli by local field potential spectra in networks of excitatory and inhibitory neurons. *PLoS Comput. Biol.* **4**, e1000239 (2008).
27. Mazzoni, A., Whittingstall, K., Brunel, N., Logothetis, N. K. & Panzeri, S. Understanding the relationships between spike rate and delta/gamma frequency bands of LFPs and EEGs using a local cortical network model. *Neuroimage* **52**, 956–972 (2010).
28. Mazzoni, A., Brunel, N., Cavallari, S., Logothetis, N. K. & Panzeri, S. Cortical dynamics during naturalistic sensory stimulations: experiments and models. *J. Physiol. Paris* **105**, 2–15 (2011).
29. Barbieri, F., Mazzoni, A., Logothetis, N. K., Panzeri, S. & Brunel, N. Stimulus dependence of local field potential spectra: experiment versus theory. *J. Neurosci.* **34**, 14589–14605 (2014).
30. Cavallari, S., Panzeri, S. & Mazzoni, A. Comparison of the dynamics of neural interactions between current-based and conductance-based integrate-and-fire recurrent networks. *Front Neural Circuits* **8**, 12 (2014).
31. Mazzoni, A. *et al.* Computing the Local Field Potential (LFP) from Integrate-and-Fire Network Models. *PLoS Comput. Biol.* **11**, e1004584 (2015).
32. Bédard, C., Kröger, H. & Destexhe, A. Does the 1/f frequency scaling of brain signals reflect self-organized critical states? *Phys. Rev. Lett.* **97**, 118102 (2006).
33. Magri, C., Schridde, U., Murayama, Y., Panzeri, S. & Logothetis, N. K. The amplitude and timing of the BOLD signal reflects the relationship between local field potential power at different frequencies. *J. Neurosci.* **32**, 1395–1407 (2012).
34. Baranauskas, G. *et al.* Origins of 1/f2 scaling in the power spectrum of intracortical local field potential. *J. Neurophysiol.* **107**, 984–994 (2012).
35. Miller, K. J., Sorensen, L. B., Ojemann, J. G. & den Nijs, M. Power-law scaling in the brain surface electric potential. *PLoS Comput. Biol.* **5**, e1000609 (2009).
36. Milstein, J., Mormann, F., Fried, I. & Koch, C. Neuronal shot noise and Brownian 1/f2 behavior in the local field potential. *PLoS ONE* **4**, e4338 (2009).
37. Leopold, D. A., Murayama, Y. & Logothetis, N. K. Very slow activity fluctuations in monkey visual cortex: implications for functional brain imaging. *Cereb. Cortex* **13**, 422–433 (2003).
38. Alexander, G. M. *et al.* Remote control of neuronal activity in transgenic mice expressing evolved G protein-coupled receptors. *Neuron* **63**, 27–39 (2009).

39. Stachniak, T. J., Ghosh, A. & Sternson, S. M. Chemogenetic synaptic silencing of neural circuits localizes a hypothalamus→midbrain pathway for feeding behavior. *Neuron* **82**, 797–808 (2014).
40. Courchesne, E. *et al.* The ASD Living Biology: from cell proliferation to clinical phenotype. *Mol. Psychiatry* **24**, 88–107 (2019).
41. Buckner, R. L. & DiNicola, L. M. The brain's default network: updated anatomy, physiology and evolving insights. *Nat. Rev. Neurosci.* **20**, 593–608 (2019).
42. Yeo, B. T. T. *et al.* The organization of the human cerebral cortex estimated by intrinsic functional connectivity. *J. Neurophysiol.* **106**, 1125–1165 (2011).
43. Kaczkurkin, A. N., Raznahan, A. & Satterthwaite, T. D. Sex differences in the developing brain: insights from multimodal neuroimaging. *Neuropsychopharmacology* **44**, 71–85 (2019).
44. Bedford, S. A. *et al.* Large-scale analyses of the relationship between sex, age and intelligence quotient heterogeneity and cortical morphometry in autism spectrum disorder. *Mol. Psychiatry* (2019) doi:10.1038/s41380-019-0420-6.
45. Livingston, L. A., Shah, P. & Happé, F. Compensatory strategies below the behavioural surface in autism: a qualitative study. *Lancet Psychiatry* **6**, 766–777 (2019).
46. Lombardo, M. V. *et al.* Atypical neural self-representation in autism. *Brain* **133**, 611–624 (2010).
47. Mitchell, J. P., Macrae, C. N. & Banaji, M. R. Dissociable medial prefrontal contributions to judgments of similar and dissimilar others. *Neuron* **50**, 655–663 (2006).
48. Robinson, E. B., Lichtenstein, P., Anckarsäter, H., Happé, F. & Ronald, A. Examining and interpreting the female protective effect against autistic behavior. *Proc. Natl. Acad. Sci. U.S.A.* **110**, 5258–5262 (2013).
49. Werling, D. M. The role of sex-differential biology in risk for autism spectrum disorder. *Biol Sex Differ* **7**, 58 (2016).
50. Lord, C., Rutter, M. & Le Couteur, A. Autism Diagnostic Interview-Revised: a revised version of a diagnostic interview for caregivers of individuals with possible pervasive developmental disorders. *J Autism Dev Disord* **24**, 659–685 (1994).
51. Baron-Cohen, S., Wheelwright, S., Skinner, R., Martin, J. & Clubley, E. The autism-spectrum quotient (AQ): evidence from Asperger syndrome/high-functioning autism, males and females, scientists and mathematicians. *J Autism Dev Disord* **31**, 5–17 (2001).
52. Lord, C. *et al.* The autism diagnostic observation schedule-generic: a standard measure of social and communication deficits associated with the spectrum of autism. *J Autism Dev Disord* **30**, 205–223 (2000).
53. Baron-Cohen, S., Wheelwright, S., Hill, J., Raste, Y. & Plumb, I. The 'Reading the Mind in the Eyes' Test revised version: a study with normal adults, and adults with Asperger syndrome or high-functioning autism. *J Child Psychol Psychiatry* **42**, 241–251 (2001).
54. Power, J. D., Barnes, K. A., Snyder, A. Z., Schlaggar, B. L. & Petersen, S. E. Spurious but systematic correlations in functional connectivity MRI networks arise from subject motion. *Neuroimage* **59**, 2142–2154 (2012).
55. Cox, R. W. AFNI: software for analysis and visualization of functional magnetic resonance neuroimages. *Comput. Biomed. Res.* **29**, 162–173 (1996).
56. Kundu, P., Inati, S. J., Evans, J. W., Luh, W.-M. & Bandettini, P. A. Differentiating BOLD and non-BOLD signals in fMRI time series using multi-echo EPI. *Neuroimage* **60**, 1759–1770 (2012).

57. Patel, A. X. *et al.* A wavelet method for modeling and despiking motion artifacts from resting-state fMRI time series. *Neuroimage* **95**, 287–304 (2014).
58. Glasser, M. F. *et al.* A multi-modal parcellation of human cerebral cortex. *Nature* **536**, 171–178 (2016).
59. Krishnan, A., Williams, L. J., McIntosh, A. R. & Abdi, H. Partial Least Squares (PLS) methods for neuroimaging: a tutorial and review. *Neuroimage* **56**, 455–475 (2011).
60. Bargiela, S., Steward, R. & Mandy, W. The Experiences of Late-diagnosed Women with Autism Spectrum Conditions: An Investigation of the Female Autism Phenotype. *J Autism Dev Disord* **46**, 3281–3294 (2016).
61. Hull, L. *et al.* 'Putting on My Best Normal': Social Camouflaging in Adults with Autism Spectrum Conditions. *J Autism Dev Disord* **47**, 2519–2534 (2017).
62. Bertero, A. *et al.* Autism-associated 16p11.2 microdeletion impairs prefrontal functional connectivity in mouse and human. *Brain* **141**, 2055–2065 (2018).
63. Gozzi, A. *et al.* A multimodality investigation of cerebral hemodynamics and autoregulation in pharmacological MRI. *Magnetic Resonance Imaging* **25**, 826–833 (2007).
64. Gutierrez-Barragan, D., Basson, M. A., Panzeri, S. & Gozzi, A. Infraslow State Fluctuations Govern Spontaneous fMRI Network Dynamics. *Curr. Biol.* **29**, 2295-2306.e5 (2019).
65. Liska, A., Galbusera, A., Schwarz, A. J. & Gozzi, A. Functional connectivity hubs of the mouse brain. *Neuroimage* **115**, 281–291 (2015).

Tables

	Time	**Condition (DREADD - SHAM)**	**Time x Condition**
Baseline	*0.82 (0.372)*	*0.81 (0.369)*	*0.36 (0.549)*
Transition	*5.65 (**0.017**)** *	*3.25 (0.081)*	4.94 (**0.026**)*
Treatment	*0.61 (0.433)*	*12.92 (**0.001**)** **	*0.66 (0.418)*

Table 1: Results from DREADD manipulation to enhance excitation. *F-statistics (p-values in parentheses) for main effects of time, condition, and time*condition interaction for each of the 3 phases of the experiment (Baseline, Transition, Treatment). * = p<0.05, ** = p<0.001.*

	Time	**Condition (DREADD - SHAM)**	**Time x Condition**
Baseline	*0.02 (0.876)*	*4.01 (0.054)*	*1.02 (0.137)*
Transition	*0.04* (0.838)	*0.35 (0.561)*	1.36 (0.243)
Treatment	*0.40 (0.533)*	*0.20* (0.673)	*0.10 (0.786)*

Table 2: Results from DREADD manipulation to enhance inhibition. *F-statistics (p-values in parentheses) for main effects of time, condition, and time*condition interaction for each of the 3 phases of the experiment (Baseline, Transition, Treatment). * = p<0.05, ** = p<0.001.*

	TD males (N=29	Autistic males (N=23)	TD females (N=33)	Autistic females (N = 25)	Sex	Diagnosis	Diagnosis * Sex Interactions
	Mean (SD)	Mean (SD)	Mean (SD)	Mean (SD)	F-statistic (p-value)	F-statistic (p-value)	F-statistic (p-value)
Age	28.00 (6.42)	27.13 (7.14)	26.99 (5.34)	27.35 (6.79)	0.1489 (0.7004)	0.0320 (0.8585)	0.2508 (0.6176)
VIQ	110.62 (11.53)	114.70 (13.04)	120.30 (10.06)	114.08 (12.79)	**5.3340 (0.02285) ***	0.3837 (0.53696)	**5.1815 (0.02484)** *
PIQ	120.00 (10.21)	114.57 (15.70)	117.39 (9.27)	110.88 (17.43)	1.4972 (0.22382)	**5.5542 (0.02027) ***	0.0453 (0.83188)
FIQ	116.97 (10.69)	116.39 (14.15)	121.45 (8.33)	114.16 (13.82)	0.4863 (0.48713)	3.3889 (0.06844)	2.2417 (0.13731)
Camouflaging Score (z-values)	-	-0.16 (0.38)	-	0.15 (0.34)		-	-
AQ	15.28 (6.99)	32.70(8.47)	11.97 (4.93)	38.44 (6.34)	0.2606 (0.61074)	300.5921 (2.2e-16)	12.4871 (0.0006)
ADI-R Reciprocal-Social-Interaction	-	17.26 (4.77)	-	16.56 (4.52)	-	-	-
ADI-R Communication	-	14.83 (3.50)	-	13.40 (3.96)	-	-	-

ADI-R Repetition	-	5.17 (2.35)	-	4.24 (1.61)	-	-	-
ADOS Communication	-	3.30 (1.74)	-	1.24 (1.30)	-	-	-
ADOS Social	-	5.48 (3.45)	-	3.48 (3.06)	-	-	-
ADOS Repetition	-	1.09 (1.12)	-	4.30 (1.61)	-	-	-
ADOS Communication + Social Total	-	8.83 (4.87)	-	4.72 (4.09)	-	-	-
RMET	27.14 (3.59)	20.83 (6.87)	28.91(2.35)	22.84 (6.40)	3.9353 (0.04989)	42.3091 (2.704e-9)	0.0166 (0.89769)
Mean FD	0.17 (0.05)	0.20 (0.07)	0.18(0.06)	0.04 (0.17)	0.5184 (0.4731)	1.7716 (0.1860)	1.1041 (0.2958)

Note: TD: Typically Developing; VIQ: verbal IQ; PIQ: performance IQ; FIQ: full-scale IQ ADI-R: Autism Diagnostic Interview–Revised; ADOS: Autism Diagnostic Observation Schedule; AQ: Autism Spectrum Quotient; RMET: Reading the Mind in the Eyes Test; FD: frame-wise displacement; *: $p < 0.05$.

Table 3. *Descriptive statistics and group comparisons for the various demographic variables.*

Parameter	Value
Population Firing Rate (E, I)	2 Hz, 5 Hz
Population Size (E, I)	8000, 2000
Resting Membrane Potential	-65 mV
Reversal Potential (AMPA, $GABA_A$)	0 mV, -80 mV
Conductance Rise Time (AMPA, $GABA_A$)	0.1 ms, 0.5 ms
Conductance Decay Time (AMPA, $GABA_A$)	2 ms, 10 ms
E:I Ratio	1:2 to 1:6

Table 4: Parameters for E:I model: *Parameters utilized in the E:I model from Gao et al.*[24]*, for simulating LFP data.*

A: Neuron model			
Parameter	**Description**	**Excitatory cells**	**Inhibitory cells**
V_{leak} (mV)	Leak membrane potential	-70	-70
$V_{threshold}$ (mV)	Spike threshold	-52	-52
V_{reset} (mV)	Reset potential	-59	-59
$\tau_{refractory}$ (ms)	Absolute refractory period	2	1
g_{leak} (nS)	Leak membrane conductance	25	20
C_m (pF)	Membrane capacitance	500	200
τ_m (ms)	Membrane time constant	20	10
B: Connection parameters			
Parameter	**Description**	**Excitatory cells**	**Inhibitory cells**
E_{AMPA} (mV)	AMPA reversal potential	0	0
E_{GABA} (mV)	GABA reversal potential	-80	-80
$\tau_{r(AMPA)}$ (ms)	Conductance rise time (AMPA)	0.4	0.2
$\tau_{d(AMPA)}$ (ms)	Conductance decay time (AMPA)	2	1
$\tau_{r(GABA)}$ (ms)	Conductance rise time (GABA)	0.25	0.25
$\tau_{d(GABA)}$ (ms)	Conductance decay time (GABA)	5	5
τ_l (ms)	Synapse latency	0	0
$g_{AMPA(rec.)}$ (nS)	AMPA conductance (recurrent)	0.178	0.233
$g_{AMPA(tha.)}$ (nS)	AMPA conductance (thalamic)	0.234	0.317
$g_{AMPA(cort.)}$ (nS)	AMPA conductance (intracortical)	0.187	0.254
g_{GABA} (nS)	GABA conductance	2.01	2.7

Table 5: Baseline reference parameters of the recurrent network model. *Parameters used in Cavallari et al.,*[30] *with conductance-based synapses.*

Supplementary Figure 1

Panels A and B show an alternative approach to enhance excitation in the recurrent network model in which an external constant current (I_e) is applied to excitatory cells. In panels C and D, a decrease of excitation in the network is simulated by decreasing the transmission probability of all recurrent synapses.

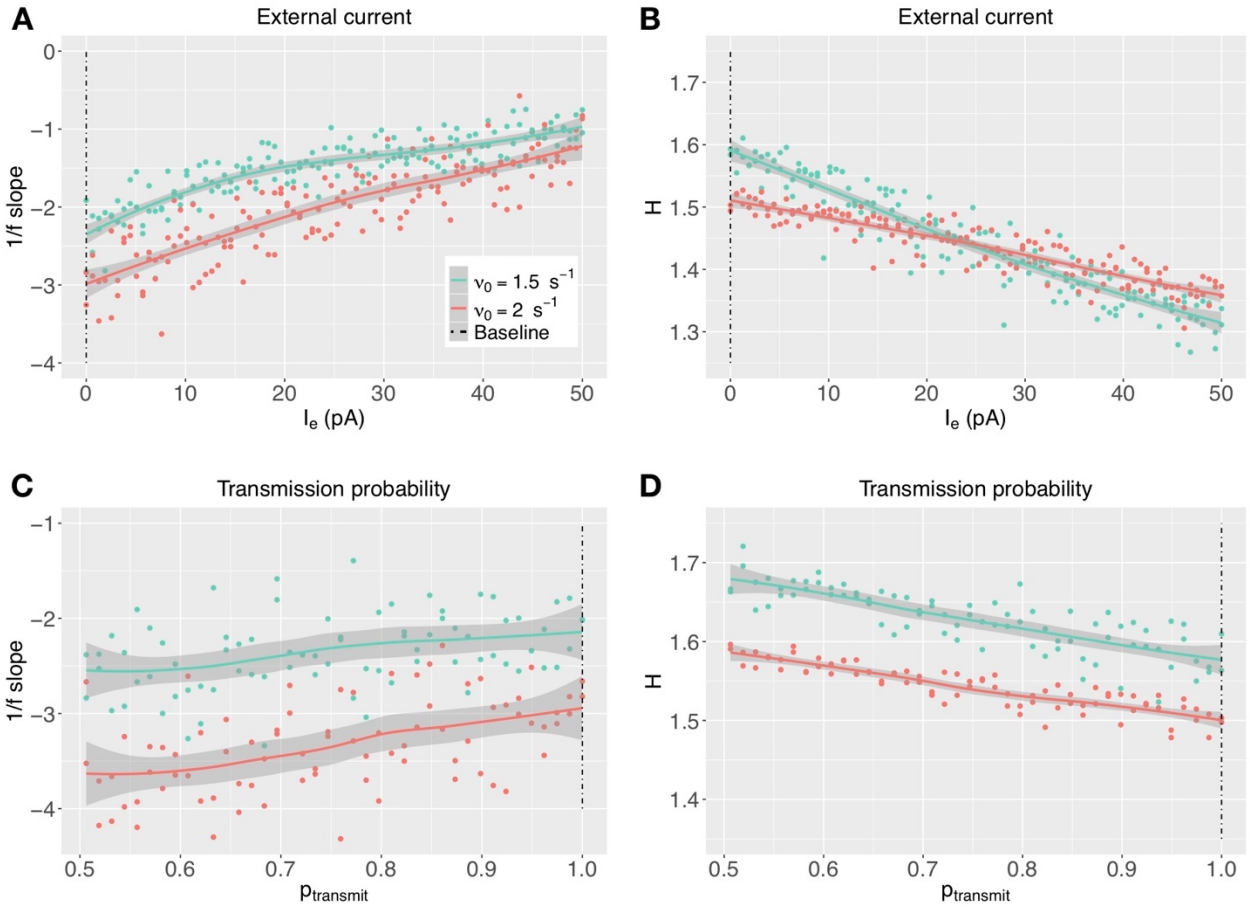

Supplementary Figure 2
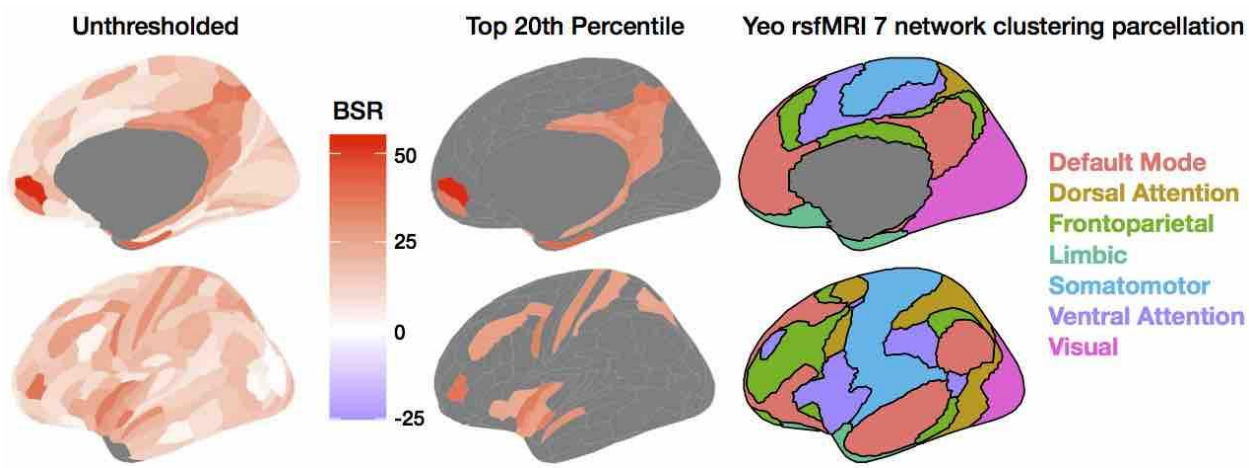
Comparison of PLS results with 7 cluster rsfMRI parcellation from Yeo et al.,[42] *which shows prominent overlap between most important PLS regions and the default mode network (DMN).*